



Fabrication and performances of solid superacid embedded chitosan hybrid membranes for direct methanol fuel cell

Jingtao Wang, Yumiao Zhang, Hong Wu, Lulu Xiao, Zhongyi Jiang*

Key Laboratory for Green Chemical Technology, School of Chemical Engineering and Technology, Tianjin University, Tianjin 300072, China

ARTICLE INFO

Article history:

Received 22 September 2009

Received in revised form

10 November 2009

Accepted 10 November 2009

Available online 14 November 2009

Keywords:

Solid superacid

Chitosan

Hybrid membrane

Free volume characteristics

Methanol permeability

Proton conductivity

ABSTRACT

This study reports the fabrication and performances of hybrid proton-conducting membranes by dispersing nanosized solid superacid inorganic fillers, $\text{TiO}_2\text{-SO}_4^{2-}$ (STiO_2), into chitosan (CS) matrix. Fourier transform infrared spectra demonstrate intermolecular interactions between STiO_2 and chitosan segmental chains. High resolution scanning electron microscope characterization reveals an essentially homogeneous dispersion of the solid superacid fillers within chitosan matrix. The incorporation of the superacid fillers leads to a reduced fractional free volume (FFV) of the hybrid membranes as confirmed by positron annihilation lifetime spectroscopy (PALS) analysis. This reduced FFV and more tortuous pathway significantly enhance the methanol diffusion resistance through the membranes, resulting in a decreased methanol crossover. Under identical conditions, compared with TiO_2 embedded membranes, the STiO_2 -filled hybrid membranes exhibit simultaneously improved methanol barrier and proton transport properties due to the enhanced interfacial interaction and proton conductive ability. Moreover, compared with Nafion 117 membrane, all the STiO_2 -filled hybrid membranes display much lower methanol crossover whereas the proton conductivity of the membranes remains high enough for DMFC applications. Meanwhile, due to the interfacial interactions between STiO_2 and chitosan chains, the hybrid membranes exhibit an enhanced mechanical strength and adequate thermal stability as verified by mechanical strength characterization and thermogravimetric analysis.

© 2009 Elsevier B.V. All rights reserved.

1. Introduction

Referred as the next generation materials, hybrid materials have been widely used in the fields of molecular recognition, biomimetics, molecular sieve, catalytic materials, membrane materials, etc. Recently, organic–inorganic hybrid membranes have been proposed as promising electrolytes for direct methanol fuel cell (DMFC) application. The rationale for incorporating the inorganic additives is manifold: (1) improving thermal, mechanical, and chemical stabilities by intrinsic organic–inorganic interfacial interactions [1,2]; (2) reducing methanol crossover through blocking methanol transport path and/or suppressing membrane swelling [3–5]; (3) enhancing proton conductivity by constructing new proton transport pathway and/or by improving water retention property of the membranes, especially, at high temperatures [6,7].

Among numerous inorganic materials, solid superacids have triggered increasing attention because of their fine hygroscopic and proton conductive properties as well as good mechanical property when incorporated into polymers, which are advantageous for high performance proton exchange membrane. To date, the

commonly-utilized solid superacids can be categorized into metal oxide supported sulfate ($\text{M}_x\text{O}_y\text{-SO}_4^{2-}$), heteropoly acid (HPA) and zeolite solid superacid [8–12]. Navarra et al. developed a high temperature superacid zirconia-doped Nafion composite membrane, and the presence of superacid promoted the hydration degree and acidity, which in turn reflected in enhanced proton conductivity ($1.5 \times 10^{-2} \text{ S cm}^{-1}$) compared with plain Nafion ($3.0 \times 10^{-6} \text{ S cm}^{-1}$) at 140°C and low relative humidity [8]. Cui et al. prepared a series of chitosan–heteropoly acids (phosphomolybdic acid, phosphotungstic acid and silicotungstic acid) hybrid membranes. They found that incorporating HPA improved both the methanol barrier and proton conductive properties [10]. Kim et al. incorporated MCM-41 supported heteropoly acid and tungstophosphoric acid (TPA) into Nafion matrix. The resulting hybrid membranes displayed higher proton selectivity and thus better DMFC performance [12].

It is well known that the solid superacid $\text{TiO}_2\text{-SO}_4^{2-}$ (STiO_2) has an acid strength stronger than that of 100% H_2SO_4 due to the presence of the promoted oxide of Lewis and Brønsted acidic sites at the surface [13–15]. Strong Lewis acidity could be attributed to the existence of unsaturated Ti^{4+} cations which bear a high electron accepting ability. It has also been proposed that the O atom in the S=O bond in SO_4^{2-} exerts pronounced inductive effects on S atom, leading to the increase of electrostatic field of Ti. As

* Corresponding author. Tel.: +86 22 23500086; fax: +86 22 23500086.
E-mail address: zhyjiang@tju.edu.cn (Z. Jiang).

for the Brønsted acidity, it could be assumed that the protonated titanium hydroxyls are rendered more acidic owing to the charge withdrawing effect of the adjacent sulfate group. In virtue of its strong acidity, $\text{TiO}_2\text{-SO}_4^{2-}$ has been widely utilized as an acid catalyst in isomerization, cracking, alkylation, acylation, esterification, etc. To our knowledge, $\text{TiO}_2\text{-SO}_4^{2-}$ has scarcely been exploited as an active inorganic filler in hybrid proton exchange membranes till now. Recently, Wu et al. have evaluated the performances of Nafion composite membranes embedded by $\text{TiO}_2\text{-SO}_4^{2-}$ and noted that in DMFC single cell performance test, the composite membrane with 6% $\text{TiO}_2\text{-SO}_4^{2-}$ content achieved similar performance at 1 M methanol feed, and a higher performance at 5 M methanol feed compared with pure Nafion membrane [16]. They also observed that the methanol crossover first decreased and then gradually increased with the filler content, in particular, these membranes displayed obvious methanol crossover (above $2.7 \times 10^{-6} \text{ cm}^2 \text{ s}^{-1}$). Furthermore, the influence of the solid superacid particle on physico-chemical properties of the composite membranes was seldom investigated. These have prompted us to extend the investigation of such inorganic material in hybrid proton exchange membrane.

In this study, chitosan (CS) was employed as a promising polymeric matrix for DMFC application considering its low cost, desirable alcohol barrier property and proton conductivity as well as adequate thermal stability after crosslinking [17–19]. Meanwhile, nanosized solid superacid $\text{TiO}_2\text{-SO}_4^{2-}$, prepared via chemical adsorption, was chosen as inorganic filler embedded into chitosan matrix to fabricate a series of hybrid proton exchange membranes for the first time. The objective was to systematically investigate the influence exerted by $\text{TiO}_2\text{-SO}_4^{2-}$ on the physico-chemical properties of membrane including mechanical strength, thermal stability, microstructure, crystallization and free volume characteristics, along with the water uptake, swelling, methanol permeability and proton conductivity of the membrane.

2. Experimental

2.1. Materials and chemicals

TiO_2 powder with 12 nm average particle diameter was supplied by zhuerna High-Tech Powder Material Co. (Shanghai, China). Chitosan (CS) with a degree of deacetylation of 91% was purchased from Golden-Shell Biochemical Co. (Zhejiang, China) and used as received. Acetic acid, sulfuric acid and methanol were of analytical grade and supplied from Tianjin. All the reagents were commercially available and used without any further purification. De-ionized water was used in all experiments.

2.2. Preparation of $\text{TiO}_2\text{-SO}_4^{2-}$

The TiO_2 nanoparticles were sulfated by chemical absorption according to the procedure in the literatures [20,21]. TiO_2 powder (10 g) was dispersed into 100 mL of 1 M H_2SO_4 aqueous solution under stirring for 4 h, then was filtrated, washed and dried in vacuum at 40 °C. Thereafter, the resultant powder was calcined at 450 °C for 4 h, and the white $\text{TiO}_2\text{-SO}_4^{2-}$ solid superacid powder was thus obtained.

2.3. Fabrication of the membranes

Chitosan (1.5 g) was dissolved in 40 mL of 2 wt.% acetic acid aqueous solution under stirring at 80 °C. Simultaneously, certain amount of TiO_2 or $\text{TiO}_2\text{-SO}_4^{2-}$ powder was dispersed into 35 mL of 2 wt.% acetic acid aqueous solution with ultrasonic treatment for 30 min. These two parts of solution were then mixed and stirred vigorously at 80 °C for another 2 h. After degasification, the resulting homogenous solution was cast onto a clear glass plate and dried

at 25 °C. The membrane was afterwards immersed and cross-linked in 2 M H_2SO_4 for 24 h and then extensively rinsed with de-ionized water to remove residual H_2SO_4 . Finally the hybrid membrane was dried under vacuum at 25 °C for 48 h. The resulting membranes were designated as CS/ TiO_2 -X or CS/ $\text{TiO}_2\text{-SO}_4^{2-}$ -X representing TiO_2 or $\text{TiO}_2\text{-SO}_4^{2-}$ as the fillers, where X (X=5, 10, 15, 20, 25 or 30) was the weight ratio of the inorganic filler to chitosan. Control CS membrane was fabricated in exactly the same way as above without incorporating inorganic filler and designated as CS. It should be pointed that membrane thickness was in range of 60–70 μm .

2.4. Characterization

The morphology of the TiO_2 before and after sulfation was characterized by transmission electron microscopy (TEM, Tecnai G20 S-TWIN). The cross-section of the membranes was observed using field emission scanning electron microscope (FESEM, Nanosem 430) operated at 5 kV after being freeze-fractured in liquid nitrogen and then sputtered with gold. The crystalline structure of the membranes was investigated with a RigakuD/max2500 v/Pc X-ray diffractometer (XRD, CuK 40Kv, 200 mV, 2° min^{-1}) in the range 3–60°. The peak position was extracted with MDIjade5 software. The Brunauer–Emmett–Teller (BET) surface area of the powder sample was determined by nitrogen adsorption on a ASAP 2020 nitrogen adsorption apparatus.

The elemental composition of the solid superacid particles was characterized by X-ray photoelectron spectroscopy (XPS) using a PHI 1600 spectrometer with an Mg K α radiation for excitation. Fourier transform infrared spectra (FTIR, 4000–400 cm^{-1}) of the fillers and membranes were recorded on a Nicolet MAGNA-IR 560 instrument. The thermogravimetric analysis (TGA, Perkin-Elmer Pyris) data of the membranes were obtained from 30 to 700 °C using a heating rate of 10 °C min^{-1} at nitrogen atmosphere. The mechanical strength of the membranes was carried out by using 350 AX overall drawing Testometric. The membranes were cut into 1.0 \times 5.0 cm for each sample and then examined with a 10 mm min^{-1} scan rate at room temperature.

Positron annihilation lifetime spectroscopy (PALS) experiment was performed by using an EG&G ORTEC fast–fast coincidence system (resolution 201 ps) at room temperature. The resource of ^{22}Na ($5 \times 10^5 \text{ Bq}$) was sandwiched between two pieces of sample, each of which with an overall thickness of about 1.0 mm. The integral statistics for each spectrum was more than 2×10^6 coincidences. In this technique, assuming that o-Ps was localized in a spherical potential well surrounded by an electron layer of thickness Δr equal to 0.1656 nm, the radius of free volume cavity (r) is obtained from pick-off annihilation lifetime (τ) of o-Ps in the free volume elements by a semiempirical equation [22,23]:

$$\tau = \frac{1}{2} \left[1 - \frac{\gamma}{\gamma + \Delta\gamma} + \left(\frac{1}{2\pi} \right) \sin \left(\frac{2\pi\gamma}{\gamma + \Delta\gamma} \right) \right]^{-1} \quad (1)$$

The volume of the equivalent sphere can be calculated by Eq. (2):

$$V_f = \frac{4\pi}{3} \gamma^3 \quad (2)$$

Further, the fractional free volume (FFV) may be estimated from Eq. (3):

$$\text{FFV} = V_f I_3 \quad (3)$$

where V_f and I are free volume of the sphere and intensity of o-Ps, respectively.

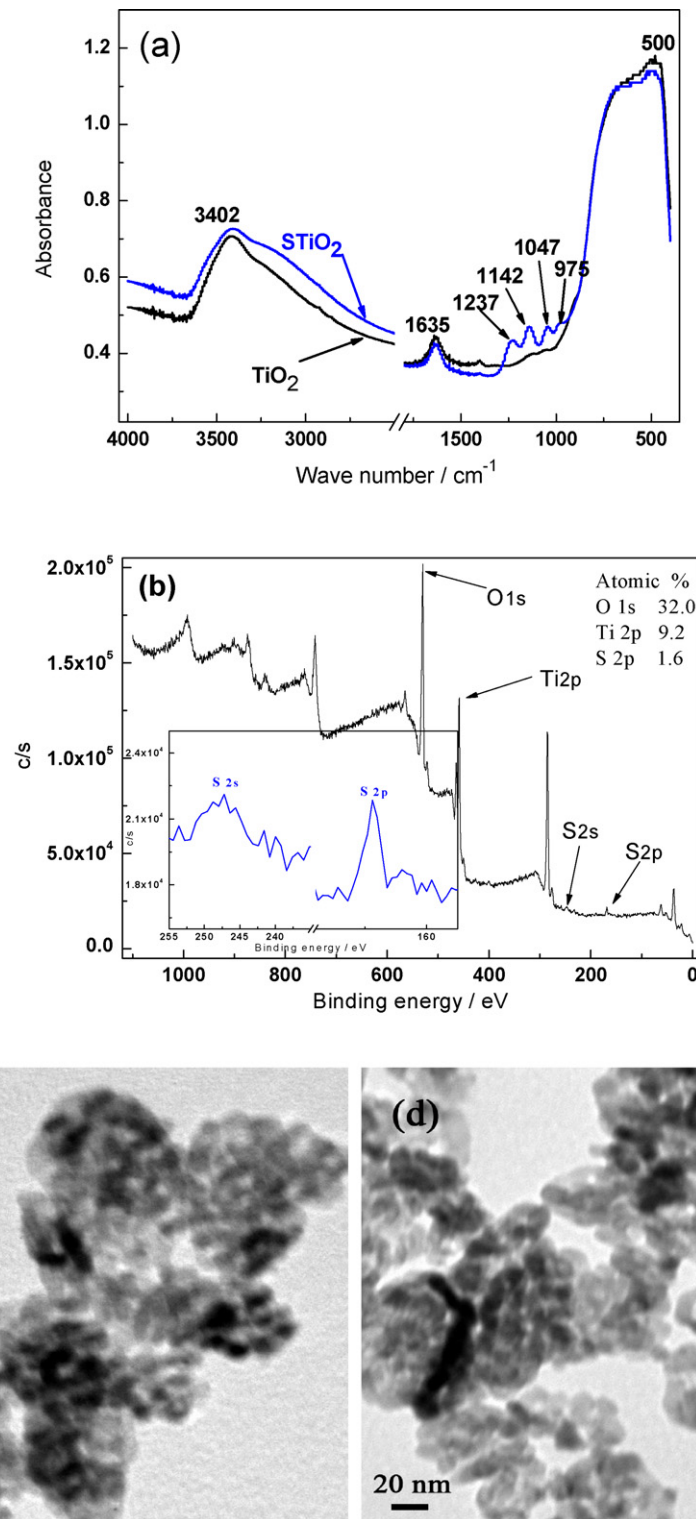


Fig. 1. Characterization of the inorganic fillers: (a) FTIR spectra, (b) XPS spectrum, (c and d) TEM images of TiO₂ and TiO₂-SO₄²⁻.

2.5. Water uptake and swelling

The water uptake of the membranes was determined as follows. The dry membrane was weighed (W_{dry}) and immersed in de-ionized water for 24 h at room temperature. Then the membrane was re-weighed (W_{wet}) quickly after removing the surface water. The surface swelling was determined in a similar method, by soaking the dry rectangular membrane (about 4.0×4.0 cm) with area

of A_{dry} in de-ionized water for 24 h, then re-measuring to obtain the wetted membrane area (A_{wet}). The final values of water uptake and swelling were the average of the three measurements with an error within $\pm 5.0\%$ and calculated by Eqs. (4) and (5), respectively:

$$\text{Water uptake}(\%) = \frac{W_{\text{wet}} - W_{\text{dry}}}{W_{\text{dry}}} \times 100 \quad (4)$$

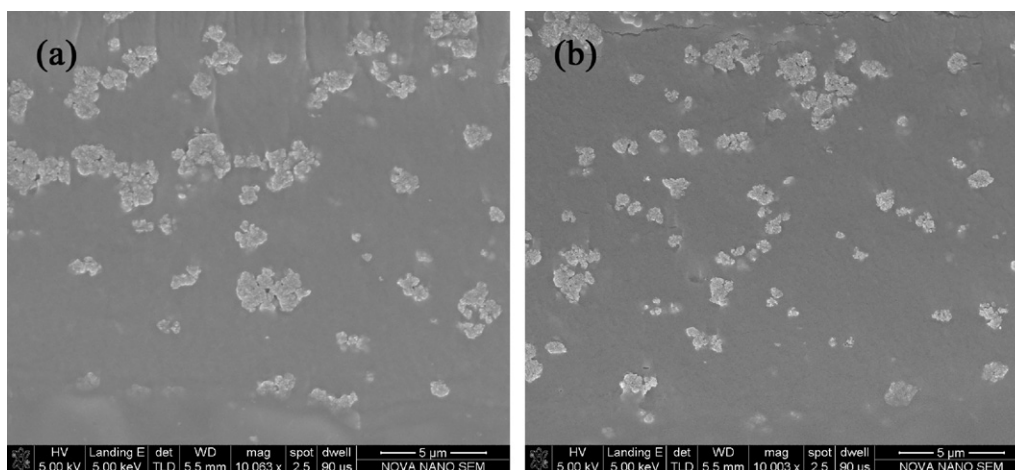


Fig. 2. FESEM images of the cross-section of the representative hybrid membranes: (a) CS/TiO₂-15 and (b) CS/STiO₂-15.

$$\text{Swelling (\%)} = \frac{A_{\text{wet}} - A_{\text{dry}}}{A_{\text{dry}}} \times 100 \quad (5)$$

2.6. Methanol permeability

The methanol permeability was measured with a glass diffusion cell as described in the literature [24], which consisted of two compartments with identical volume separated by a membrane sheet. The membrane was hydrated in de-ionized water for 24 h before being clamped tightly between the two compartments, one of which was initially filled with water and the other filled with 2.0 M methanol solution. The methanol concentration in the receipt compartment was determined using a gas chromatography (Agilent 6820) equipped with a TCD detector and a DB624 column. The methanol permeability (P , cm² s⁻¹) was calculated from Eq. (6):

$$P = S \frac{V_B l}{AC_{A0}} \quad (6)$$

where S is the slope of the straight line of concentration versus time, V_B is the volume of the receipt compartment, l , A , and C_{A0} are the membrane thickness, effective membrane area, and feed concentration, respectively. The measurement error was within $\pm 4.0\%$.

2.7. Proton conductivity

The proton conductivity of the membranes in the transverse direction was measured in two-point-probe conductivity cells by the ac impedance spectroscopy method over a frequency range of 1–10⁶ Hz with oscillating voltage of 20 mV, using a frequency response analyzer (FRA, Compactstat, IVIUM Tech.) at 20 \pm 1 °C. All the membrane samples were immersed in 0.2 M H₂SO₄ for 24 h prior to measurement in order to eliminate the contact resistance between 316L electrode and membrane surface, which was similar to the treatment in the literature [1,24]. The proton conductivity (σ , S cm⁻¹) of the sample in transverse direction was the average of the three measurements with an error within $\pm 4.5\%$ and calculated by Eq. (7):

$$\sigma = \frac{l}{AR} \quad (7)$$

where l and A are membrane thickness and membrane area, respectively, and R is the membrane resistance obtained from the FRA.

3. Results and discussion

3.1. Characterization of TiO₂-SO₄²⁻

The FTIR spectrum was utilized to determine the chemical structure of the inorganic fillers qualitatively as shown in Fig. 1a. According to the spectra, a strong peak at around 500 cm⁻¹ was observed due to the vibration of the bonding of Ti–O together with the two peaks around 3402 and 1635 cm⁻¹ were mainly attributed to stretching and deformation vibration of the adsorbed water, respectively [20]. After sulfation, the introduction of the sulfate groups was definitely verified by the appearance of four new peaks around 1237, 1142, 1047 and 975 cm⁻¹ that were attributed to the stretching vibration of the S=O bond or S–O bond. Based on the previous studies, the three peaks at 1237, 1142 and 1047 cm⁻¹ were characteristic of chelating bidentate SO₄²⁻, and unidentate SO₄²⁻ exhibited two bands at 1142 and 975 cm⁻¹ [20,25]. Accordingly, both chelating ligand structure and bridged coordination were formed between TiO₂ and sulfate group. In general, the high wave number was the characteristic of superacidic property of M_xO_y-SO₄²⁻ mode and accordingly, the appearance of the peak at 1237 cm⁻¹ indicated that the solid superacid TiO₂-SO₄²⁻ was acquired successfully. Meanwhile, the intensity of water peak at 3402 cm⁻¹ became stronger after sulfation due to its hygroscopic property, implying an enhanced hydrophilicity of the particles, which may facilitate the proton transport. For further quantitative characterization, the XPS spectrum as presented in Fig. 1b exhibited the peak of binding energy around 247.5 and 168.7 eV corresponding to the S 2s and S 2p, respectively, indicating the S atom was in typical hexed-oxidation state (S⁶⁺) of sulfate [20,26]. In addition, according to the spectrum, the atomic percentages of Ti and S were 9.2% and 1.6%, respectively and it could be calculated that the surface content of SO₄²⁻ in particle was about 7.15% in weight.

Meanwhile, the microstructure of the TiO₂ before and after sulfation was determined by TEM and BET analysis. TEM image shown in Fig. 1c revealed that the particle size of TiO₂ powder was about 12 nm. After sulfation, the crystalline size was reduced to about 10 nm (Fig. 1d), suggesting that the addition of sulfate ions into TiO₂ particles might retard the crystallization during the calcination procedure, which was in agreement with the literature [27]. This can also be confirmed by BET analysis. An increasing BET surface area from 110.6 m² g⁻¹ for TiO₂ particles to 127.8 m² g⁻¹ for STiO₂ particles was observed after acid modification. Collectively, these data confirmed that the solid superacid STiO₂ particles with 10 nm diameter were successfully prepared, which endowed the possi-

bility to tailor the membrane performance by embedding these inorganic particles into polymer matrix.

3.2. Characterization of CS/STiO₂ hybrid membranes

The internal morphologies and the miscibility of organic and inorganic phase were investigated by FESEM and Fig. 2a and b exhibited the representative cross-section images of the hybrid membranes containing 15% TiO₂ and STiO₂ fillers, respectively. According to Fig. 2a, obvious TiO₂ aggregation (around 2.0 μm aggregate size) could be observed, which was reasonably attributed to their high surface tension and poor interfacial compatibility with bulk polymer. After sulfation, the interfacial compatibility would be improved owing to the enhanced hydrophilicity and interfacial interaction between STiO₂ and chitosan chains. The aggregation of STiO₂ particles became less (around 1.0 μm aggregate size), and therefore the particles displayed better dispersion within bulk chitosan compared with TiO₂ particles, as shown in Fig. 2b. The better dispersion would produce more effective polymer/particle interfacial area, and offer more possibility of surface-induced tailoring of the structure, hence potentially improving the membrane performance.

To systematically investigate the influence of the solid superacid fillers on the physicochemical properties of the hybrid membranes, FTIR, XRD, TGA and mechanical strength characterizations were utilized and the results were illustrated in Figs. 3–6, respectively. FTIR spectra have been employed to get a better understanding of the interfacial interaction between the fillers and chitosan matrix. According to the spectra in Fig. 3, all the samples possessed three characteristic peaks at 3247, 1642 and 1536 cm⁻¹, which were assigned to the vibration of the hydroxyl, amide I and amide II groups on the chitosan chains, respectively. After STiO₂ incorporation, the absorption intensities of these characteristic peaks became weaker and followed the order of CS > CS/STiO₂-10 > CS/STiO₂-20 > CS/STiO₂-30. Such observations were reasonably originated from the formation of interfacial interactions including: (i) hydrogen-bonding interactions between S=O of inorganic fillers and the amide or hydroxyl groups of chitosan chains; (ii) electrostatic interactions between SO₄²⁻ of TiO₂-SO₄²⁻ and ⁺H₃N- from amino groups protonation in acetic acid solution during membrane preparation. Consequently, the free hydroxyl and amide groups of chitosan decreased, hence weakening the intensities of the characteristic peaks.

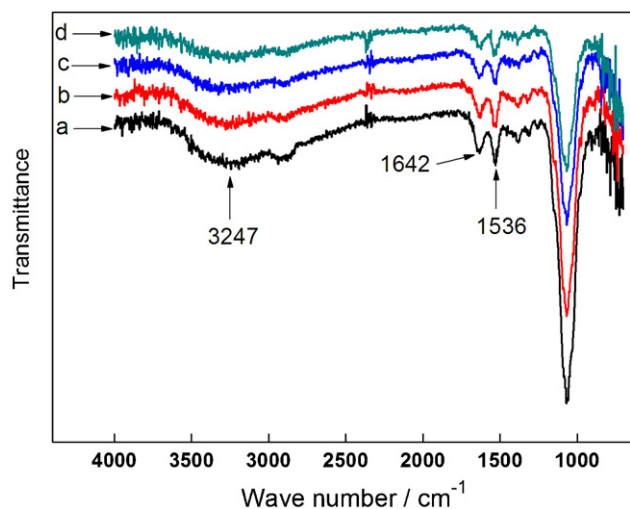


Fig. 3. FTIR spectra of CS and hybrid membranes: (a) CS, (b) CS/STiO₂-10, (c) CS/STiO₂-20 and (d) CS/STiO₂-30.

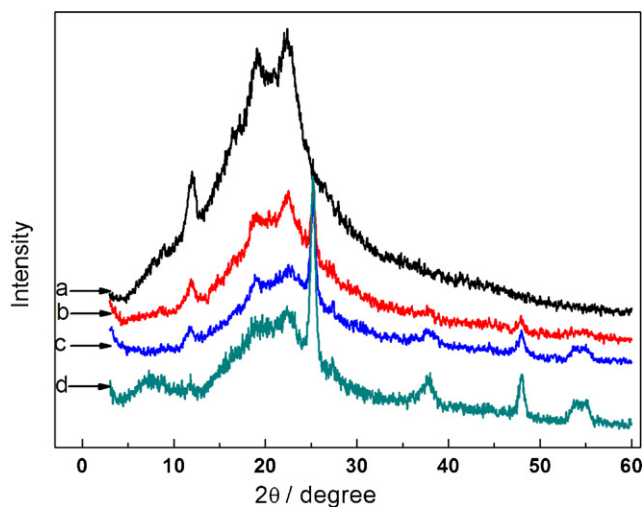


Fig. 4. XRD patterns of (a) CS, (b) CS/STiO₂-10, (c) CS/STiO₂-20 and (d) CS/STiO₂-30 membranes.

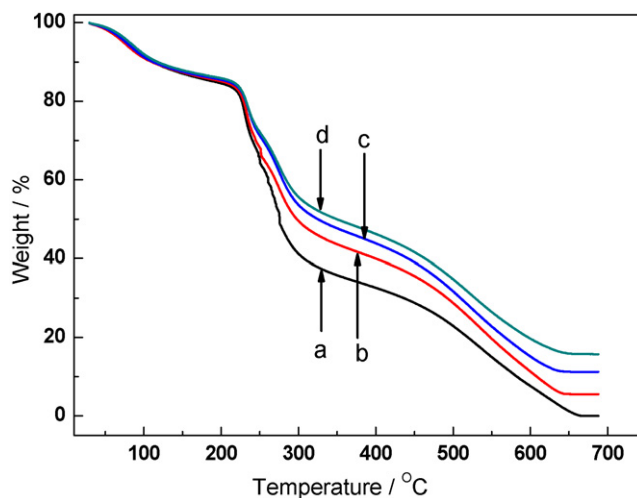


Fig. 5. TGA thermodiagram of CS and hybrid membranes: (a) CS, (b) CS/STiO₂-10, (c) CS/STiO₂-20 and (d) CS/STiO₂-30.

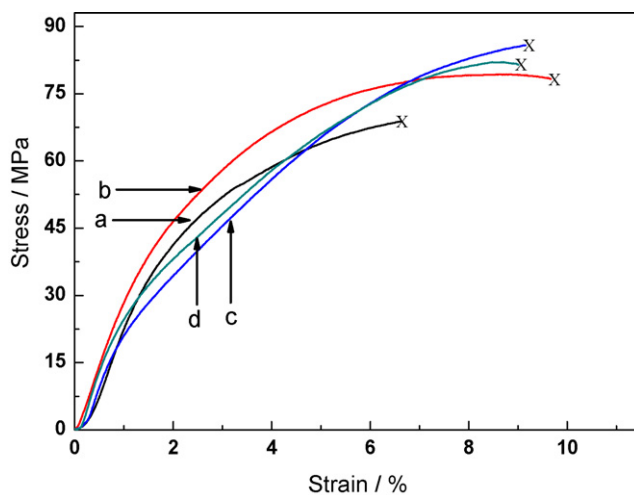


Fig. 6. Stress–strain curves of (a) CS, (b) CS/STiO₂-10, (c) CS/STiO₂-20 and (d) CS/STiO₂-30 membranes.

The XRD patterns of control membrane and CS/STiO₂ hybrid membranes were presented in Fig. 4 to evaluate the influence of inorganic fillers on crystalline structures of chitosan matrix. In agreement with the observation in the literature [28], the control membrane (Fig. 4a) exhibited three characteristic peaks at $2\theta = 11.8^\circ$, 18.8° , 21.6° and some other diffraction peaks due to the semicrystalline character of chitosan. For the hybrid membranes, the incorporation of inorganic fillers interfered with the ordered packing of the chitosan chains by steric effects and the interfacial interactions, thus destroying the crystalline domain of chitosan matrix. Accordingly, as shown in Fig. 4b–d, the peak intensity of the chitosan became weaker with the increase of the STiO₂ content. In addition, the new peaks in XRD patterns of the hybrid membranes at around $2\theta = 25.1^\circ$, 27.4° , 37.8° , 47.9° and 54.8° were attributed to the crystalline structure of inorganic filler [29], the intensities of which increased with the filler content as shown in Fig. 4b–d.

Thermal stability of the control and hybrid membrane samples could be referred from their TGA thermograms as presented in Fig. 5. In consistence with previous study [30], all the membranes would undergo three-step weight loss stage as follows: (i) water evaporation from membrane phase around 50–100 °C; (ii) degradation of chitosan chains around 220–310 °C; (iii) final membrane matrix degradation around 480–650 °C. It could be calculated that the values of char yields (5.46% for CS/STiO₂-10, 11.28% for CS/STiO₂-20 and 16.04% for CS/STiO₂-30) were around 65% of the amount of the STiO₂ fillers arising from the loss of sulfate acid groups and adsorbed water. These observations suggested that the increased char ratios were mainly ascribed to the nonvolatile inorganic fillers and not to the chitosan matrix. Accordingly, it can be conjectured that the thermal degradation mechanism of chitosan might remain unchanged by the embedded fillers. Similar results were also reported for other composite membranes [30,31]. Moreover, it should be noted that the membrane matrix began to degrade at about 220 °C, indicating that the membrane could retain its thermal stability at practical operating temperature (<100 °C) for DMFC application.

Fig. 6 presented the mechanical strength characterization of the control chitosan and hybrid membranes with different STiO₂ content. Compared to control membrane (Fig. 6a), an improvement in mechanical strength was probed for hybrid membranes (Fig. 6b–d), exhibiting tensile strength values of 78.80 MPa for CS/STiO₂-10, 85.77 MPa for CS/STiO₂-20 and 81.83 MPa for CS/STiO₂-30, which were 14.1%, 24.2% and 18.5% higher than that of the control membrane (69.06 MPa), respectively. However, when the loading of fillers exceeded to a certain amount, reduction (decreasing from 85.77 MPa for CS/STiO₂-20 to 81.83 MPa for CS/STiO₂-30) in tensile strength was observed owing to the formation of unexpected non-ideal voids caused by the aggregation of the inorganic fillers. In addition, the hybrid membrane displayed an increasing elongation (above 9.0%) compared with control chitosan membrane (6.6%), indicating that the addition of STiO₂ particles significantly enhanced the flexibility of the membrane.

3.3. Free volume characteristics analysis and methanol permeability evaluation of the membrane

3.3.1. Free volume characteristics

Free volume characteristics, as an effective direct parameter for describing the morphology of the membrane, could reflect the mobility and packing of polymer chains. Since the transport of methanol within DMFC membrane can be described by solution-diffusion mechanism, in which the process is dominated by the diffusivity of methanol in most cases [32,33], the nanoscale morphology would strongly determine the transport properties of a DMFC membrane. So it is necessary to gain a deeper understand-

Table 1
Free volume parameters of the as-prepared membranes.

Entry	Membrane	τ_3 (ns)	I_3 (%)	r_3 (nm)	V_f (nm ³)	FFV (%)
1	CS	1.985	15.55	0.2835	0.0954	1.483
2	CS/STiO ₂ -5	1.968	15.46	0.2819	0.0938	1.450
3	CS/STiO ₂ -10	1.952	15.39	0.2804	0.0923	1.420
4	CS/STiO ₂ -15	1.947	15.43	0.2799	0.0918	1.417
5	CS/STiO ₂ -20	1.940	15.22	0.2792	0.0911	1.389
6	CS/STiO ₂ -25	1.943	15.31	0.2795	0.0914	1.399
7	CS/STiO ₂ -30	1.966	15.20	0.2817	0.0936	1.423
8	CS/TiO ₂ -5	1.976	15.60	0.2826	0.0945	1.474
9	CS/TiO ₂ -10	1.962	15.42	0.2814	0.0933	1.439
10	CS/TiO ₂ -15	1.950	15.30	0.2802	0.0921	1.409
11	CS/TiO ₂ -20	2.022	14.68	0.2868	0.0988	1.449
12	CS/TiO ₂ -25	2.035	14.91	0.2880	0.1001	1.491
13	CS/TiO ₂ -30	2.054	14.81	0.2897	0.1018	1.508

ing of the influence exerted by inorganic fillers on the free volume characteristics in hybrid membranes.

PALS technique was employed to measure the free volume characteristics and the corresponding parameters of the as-prepared membranes were tabulated in Table 1. According to the τ_3 parameter, free volume cavities in control chitosan membrane possessed (Entry 1) an average radius about 0.284 nm, which was consistent with our previous study [28]. Compared with control membrane, the addition of TiO₂ reduced the average radius of free volume cavities when filler content was less than 15% (Entries 8–10), which was due to the hydrogen-bonding interactions between chitosan and particles, inhibiting the matrix chains mobility and promoting the stress at the interface and rigidification of chitosan chains near the interfacial regions. However, when excessive fillers (above 15%, entries 11–13) were impregnated, the average cavity size in hybrid membranes increased from 0.280 to 0.290 nm. The increase of radius should be attributed to the formation of non-selective voids, and similar results were also reported for other hybrid membranes [34]. The similar changing trend (the cavities first became smaller and then larger with the increase of fillers content) was observed for CS/STiO₂ membrane (Entries 2–7). Meanwhile, under the same amount of fillers, STiO₂ filled membrane displayed smaller average cavity size than TiO₂ filled membrane as a result of the enhanced interfacial interactions between the inorganic fillers and chitosan chains. The fractional free volume (FFV parameter in Table 1), which influenced the mass diffusion through the free volume cavities, of the hybrid membranes (Entries 2–11) was smaller than that of control chitosan membrane (Entry 1), which might therefore facilitate to suppress methanol crossover of the membranes according to Fujita free volume theory [35]. The results of free volume characteristics were in good agreement with FTIR, TGA and mechanical strength characterizations.

3.3.2. Water uptake, swelling and methanol permeability

Table 2 summarized the data of water uptake, swelling and methanol permeability of a Nafion 117, control CS membrane, CS/STiO₂ and CS/TiO₂ membranes. Water uptake, influencing proton conductivity and membrane-catalyst interface directly, was an important parameter in view of fuel cell applications [36]. It is well known that the adsorbed water mainly located surrounding the hydrophilic groups of chitosan chains whereas the dense inorganic fillers made a negligible contribution to the total water uptake. Therefore, the hybrid membranes (Water uptake parameter in Table 2, entries 3–14) exhibited lower water uptake than control CS membrane (Entry 2), and it decreased further with the filler content owing to the reduction of chitosan mass percentage in per unit weight. In addition, compared with CS/TiO₂ membranes, the TiO₂-SO₄²⁻ embedded hybrid membranes displayed lower fractional free volume and less non-selective voids for accommodating water molecules as testified by PALS and FESEM characterizations,

Table 2

Water uptake, swelling and methanol permeability of a Nafion 117, CS and the hybrid membranes.

Entry	Membrane	Water uptake (%)	Swelling (%)	Methanol permeability ($10^{-7} \text{ cm}^2 \text{ s}^{-1}$)
1	Nafion 117	30.55	37.56	31.54
2	CS	64.94	46.91	11.64
3	CS/STiO ₂ -5	57.44	41.70	7.62
4	CS/STiO ₂ -10	55.43	39.93	6.48
5	CS/STiO ₂ -15	52.90	37.24	5.97
6	CS/STiO ₂ -20	49.27	36.77	5.68
7	CS/STiO ₂ -25	48.16	36.26	5.56
8	CS/STiO ₂ -30	47.38	34.86	5.69
9	CS/TiO ₂ -5	59.14	44.47	8.09
10	CS/TiO ₂ -10	56.88	43.64	8.04
11	CS/TiO ₂ -15	56.07	41.03	7.76
12	CS/TiO ₂ -20	54.26	38.17	6.80
13	CS/TiO ₂ -25	53.36	37.63	7.35
14	CS/TiO ₂ -30	50.64	35.93	8.12

and hence exhibited a reducing water uptake under the same filler content. Since both swelling and water uptake of these membranes were mainly caused by the water adsorption in bulk polymer, the results of swelling were quite consistent with that of water uptake. In other words, the high swelling degree of the membrane was acquired via a high water uptake.

Previous studies have demonstrated that the free volume cavities could provide diffusing molecules with a low-resistance path for transport, and penetrant-transporting through a dense membrane is mainly determined by diffusing in the free volume cavities [37]. According to Table 1, the average radius of free volume cavities in the control chitosan and hybrid membranes (about 0.28 nm) were larger than the kinetic radius of methanol molecule (0.19 nm), indicating that the methanol transporting through the membrane would occur in these cavities. Nafion 117, commonly used in the DMFC for its high proton conductivity, showed serious methanol crossover ($3.15 \times 10^{-6} \text{ cm}^2 \text{ s}^{-1}$) under identical conditions. By comparison, the as-prepared membranes displayed fine methanol barrier property according to the methanol permeability parameter in Table 2. It was clear that after incorporation of inorganic fillers, the methanol resistance property of the membrane was obviously improved originating from the non-permeable particles which reduced the fractional free volume (*FFV* parameter in Table 1) as well as obstructed the methanol transport hence inducing tortuous pathway for methanol. Table 2 revealed that the CS/STiO₂ membranes exhibited lower methanol crossover than CS/TiO₂ membranes. Such phenomena were ascribed to the facts as follows: (i) inorganic fillers were dispersed more homogeneously in the polymer matrix after sulfation as testified by FESEM analysis, which more effectively lengthened the methanol diffusion pathway; (ii) TiO₂-SO₄²⁻ exhibited better interfacial compatibility with chitosan matrix to reduce the non-selective voids; (iii) CS/STiO₂ membrane possessed lower fractional free volume as shown in Table 1, which all increased the diffusion resistance for methanol molecules through the membrane. It was pointed out that excessive loading of inorganic fillers would lead to the increase of methanol permeability (Entries 8, 13 and 14) caused by the formation of too many non-selective voids as mentioned above.

3.4. Proton conductivity and comprehensive performance evaluation

The proton conductivity of the membrane is of particular importance and plays a significant role for the performance of a DMFC. Higher levels of proton conductivity result in higher operational fuel cell voltage and power densities. Proton migration in polymer electrolyte membrane is well studied and discussed in the

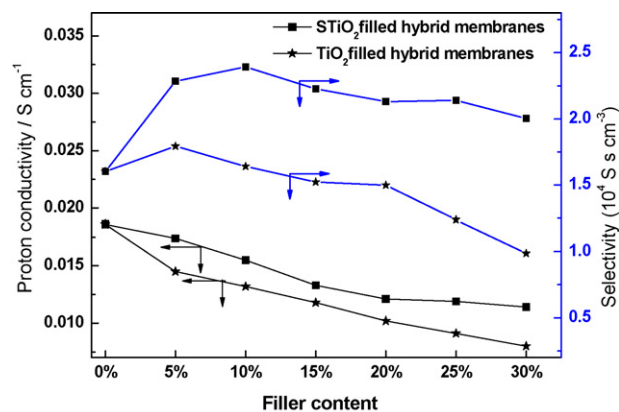


Fig. 7. Proton conductivity and selectivity of control CS and hybrid membranes as a function of filler content.

view of a vehicle mechanism (protons diffuse accompanying water molecules) and a Grotthuss mechanism (protons hop from one site to a neighboring one), which both exist in chitosan-based membranes [17,38]. The proton conductivity results in the transverse direction listed in Fig. 7 indicated that control chitosan membrane exhibited desirable proton conductivity (0.0183 S cm^{-1}) owing to its proton-conducting groups as well as the high water uptake. For CS/TiO₂ hybrid membranes, the incorporation of the fillers for one thing reduced the water content (testified by water uptake analysis) which was disadvantageous to proton transport by vehicle mechanism, and for another, it lengthened the transport pathway and increased the conductive resistance due to the presence of the less-conductive particles. Accordingly, compared with control membrane, lower proton conductivity was observed after embedding TiO₂ fillers, which decreased gradually from 0.0145 to 0.008 S cm^{-1} as the filler content increased from 5% to 30%. After sulfation, the hydrophilicity of the inorganic fillers was enhanced due to the presence of acid groups on the particle surface which would facilitate to form more hydrogen-bonded network, meanwhile it possessed proton carriers including $-\text{SO}_4^{2-}$ and $-\text{SOH}$ groups. Both of these were advantageous to proton migration, and an enhancement in proton conductivity was correspondingly observed compared with TiO₂ incorporated membranes under the same filler content. It should be pointed out that the proton conductivity of CS and CS/STiO₂ membranes (in range of 0.0114 – 0.0186 S cm^{-1}), although much lower than that of Nafion 117 (0.064 S cm^{-1}), was still high enough ($>0.01 \text{ S cm}^{-1}$) to serve as the proton exchange membrane for DMFC applications [39].

The comprehensive performance of the membrane was reflected by selectivity S , where $S = \sigma/P$ with the proton conductivity σ and methanol permeability P [40]. It was found that the methanol permeability of the membranes immersed in 0.2 M sulfuric acid was quite close to (within 3.5%) that in water, and therefore, the data of methanol permeability obtained by immersing in water were employed to calculate the selectivity data. As shown in Fig. 7, the incorporation of moderate loading TiO₂ fillers could enhance comprehensive performance of chitosan membrane. While excessive addition of TiO₂ particles (above 10%) would reduce the selectivity of the hybrid membrane as a result of the serious reduction of proton conductive property. Due to the simultaneously enhanced methanol barrier and proton conductive properties, CS/STiO₂ membranes exhibited higher comprehensive performance than CS/TiO₂ membranes. It should be pointed out that the selectivity of all the CS/STiO₂ membranes was higher than that of control CS membrane and the selectivity of CS/STiO₂-10 ($2.40 \times 10^4 \text{ S s cm}^{-3}$) was 49.1% higher than that of control CS membrane ($1.61 \times 10^4 \text{ S s cm}^{-3}$).

4. Conclusions

Nanosized solid superacid $\text{TiO}_2\text{-SO}_4^{2-}$ was synthesized via chemical absorption of commercial TiO_2 particles and then incorporated into chitosan matrix to fabricate hybrid membranes for direct methanol fuel cell application. The influence exerted by $\text{TiO}_2\text{-SO}_4^{2-}$ on the physicochemical properties of the hybrid membranes was investigated by FTIR, FESEM, XRD, TGA, PALS and mechanical strength characterizations. The presence of solid superacid fillers inhibited the chitosan chain mobility through the interfacial interactions between the fillers and chitosan chains, and thus led to enhanced mechanical strength and thermal stability. Meanwhile, the presence of the TiO_2 or STiO_2 particles within chitosan matrix induced a reduction of fractional free volume as well as a more tortuous diffusion pathway for methanol molecules, which both enhanced the methanol diffusion resistance and therefore significantly reduced methanol crossover through the membrane. The proton conductivity of the membrane decreased with the incorporation of TiO_2 particles due to the presence of the less-conductive particles, which prolonged the transport pathway and increased the conductive resistance. Upon sulfation, due to the ameliorative hygroscopic and proton conductive properties, the STiO_2 embedded hybrid membranes displayed a higher proton conductivity compared with TiO_2 embedded membranes. Consequently, CS/ STiO_2 hybrid membranes acquired higher selectivity compared with control chitosan membrane.

Acknowledgement

We gratefully acknowledge financial support from the National Nature Science Foundation of China (No. 20776101), the Programme of Introducing Talents of Discipline to Universities (No. B06006), the Program for Changjiang Scholars and Innovative Research Team in University from the Ministry of Education of China and The Project-sponsored by SRF for ROCS, SEM.

References

- [1] S.P. Jiang, Z. Liu, Z.Q. Tian, *Adv. Mater.* 18 (2006) 1068–1072.
- [2] Y.F. Lin, C.Y. Yen, C.H. Hung, Y.H. Hsiao, C.C.M. Ma, *J. Power Sources* 168 (2007) 162–166.
- [3] R.H. He, Q.F. Li, G. Xiao, N.J. Bjerrum, *J. Membr. Sci.* 226 (2003) 169–184.
- [4] J.D. Kim, T. Mori, I. Honma, *J. Electrochem. Soc.* 153 (2006) A508–A514.
- [5] S.R. Narayanan, S.P. Yen, L. Liu, S.G. Greenbaum, *J. Phys. Chem. B* 110 (2006) 3942–3948.
- [6] W.F. Chen, J.S. Wu, P.L. Kuo, *Chem. Mater.* 20 (2008) 5756–5767.
- [7] J.M. Thomassin, J. Kollar, G. Caldarella, A. Germain, R. Jérôme, C. Detrembleur, *J. Membr. Sci.* 303 (2007) 252–257.
- [8] M.A. Navarra, F. Croce, B. Scrosati, *J. Mater. Chem.* 17 (2007) 3210–3215.
- [9] S.Z. Ren, G.Q. Sun, C.N. Li, S.Q. Song, Q. Xin, X.F. Yang, *J. Power Sources* 157 (2006) 724–726.
- [10] Z.M. Cui, W. Xing, C.P. Liu, J.H. Liao, H. Zhang, *J. Power Sources* 188 (2009) 24–29.
- [11] J.L. Malers, M.A. Sweikart, J.L. Horan, J.A. Turner, A.M. Herring, *J. Power Sources* 17 (2007) 83–88.
- [12] Y.C. Kim, J.Y. Jeong, J.Y. Hwang, S.D. Kim, S.C. Yi, W.J. Kim, *J. Membr. Sci.* 325 (2008) 252–261.
- [13] V. Bolis, G. Magnacca, G. Cerrato, C. Morterra, *Langmuir* 13 (1997) 888–894.
- [14] J.H. Lunsford, H. Sang, S.M. Campbell, C.H. Liang, R.G. Anthony, *Catal. Lett.* 27 (1994) 305–314.
- [15] A. Coma, *Chem. Rev.* 95 (1995) 559–614.
- [16] Z.M. Wu, G.Q. Sun, W. Jin, H.Y. Hou, S.L. Wang, Q. Xin, *J. Membr. Sci.* 313 (2008) 336–343.
- [17] J. Ramírez-Salgado, *Electrochim. Acta* 52 (2007) 3766–3778.
- [18] B.P. Tripathi, V.K. Shahi, *J. Phys. Chem. B* 112 (2008) 15678–15690.
- [19] P. Mukoma, B.R. Jooste, H.C.M. Vosloo, *J. Power Sources* 136 (2004) 16–23.
- [20] B. Wang, W. Mao, H.Z. Ma, *Ind. Eng. Chem. Res.* 48 (2009) 440–445.
- [21] X.C. Wang, J.C. Yu, P. Liu, X.X. Wang, W.Y. Su, X.Z. Fu, *J. Photochem. Photobiol. A: Chem.* 179 (2006) 339–347.
- [22] P. Winberg, K. DeSitter, C. Dotremont, S. Mullens, I.F.J. Vankelecom, F.H.J. Maurer, *Macromolecules* 38 (2005) 3776–3782.
- [23] M. García, J. Barsema, R.E. Galindo, D. Cangialosi, J. Garcia-Turiel, W.E. VanZyl, H. Verweij, D.H.A. Blank, *Polym. Eng. Sci.* 44 (2004) 1240–1246.
- [24] B. Libby, W.H. Smyrl, E.L. Cussler, *AIChE J.* 49 (2003) 991–1001.
- [25] Y.H. Xu, L.Y. Wang, Q. Zhang, S.J. Zheng, X.J. Li, C. Huang, *Mater. Chem. Phys.* 92 (2005) 470–474.
- [26] Q.J. Yang, C. Xie, Z.L. Xu, Z.M. Gao, Y.G. Du, *J. Phys. Chem. B* 109 (2005) 5554–5560.
- [27] F. Jiang, Z. Zheng, Z.Y. Xu, S.R. Zheng, Z.B. Guo, L.Q. Chen, *J. Hazard. Mater.* 134 (2006) 94–103.
- [28] J. Wang, X. Zheng, H. Wu, B. Zheng, Z. Jiang, X. Hao, B. Wang, *J. Power Sources* 178 (2008) 9–19.
- [29] H.X. Li, G.S. Li, J. Zhu, Y. Wan, *J. Mol. Catal. A: Chem.* 226 (2005) 93–100.
- [30] Y.L. Liu, C.Y. Hsu, Y.H. Su, J.Y. Lai, *Biomacromolecules* 6 (2005) 368–373.
- [31] T. Kashiwagi, A.B. Morgan, J.M. Antonucci, M.R. VanLandingham, R.H. Harris Jr., W.H. Awad, J.R. Shields, *J. Appl. Polym. Sci.* 89 (2003) 2072–2078.
- [32] N. Miyake, J.S. Wainright, R.F. Savinell, *J. Electrochem. Soc.* 148 (2001) A905–A909.
- [33] Z.X. Liang, T.S. Zhao, J. Prabhuram, *J. Membr. Sci.* 283 (2006) 219–224.
- [34] W. Yuan, W. Hong, Z. Bin, Z. Hong, Z. Jiang, X. Hao, B. Wang, *J. Power Sources* 172 (2007) 604–612.
- [35] H. Fujita, *Fortschr. Hochpolym. Forsch.* 3 (1961) 1–47.
- [36] C. Bi, H.M. Zhang, Y. Zhang, X.B. Zhu, Y.W. Ma, H. Dai, S.H. Xiao, *J. Power Sources* 184 (2008) 197–203.
- [37] J. Wang, H. Zhang, Z. Jiang, X. Yang, L. Xiao, *J. Power Sources* 188 (2009) 64–74.
- [38] B. Smitha, S. Sridhar, A.A. Khan, *Macromolecules* 37 (2004) 2233–2239.
- [39] V. Neburchilov, J. Martin, H. Wang, J. Zhang, *J. Power Sources* 169 (2007) 221–238.
- [40] D.K. Kim, G.P. Robertson, M.D. Guiver, *Macromolecules* 41 (2008) 2126–2134.